

Model predictive control of wakes for wind farm power tracking

Arnold Sterle, Christian A. Hans, Jörg Raisch

This work was partially supported by the German Federal Ministry for Economic Affairs and Climate Action (BMWK), project No. 03EE2036C.

A. Sterle and J. Raisch are with Technische Universität Berlin, Control Systems Group, Germany. J. Raisch is also with Science of Intelligence, Research Cluster of Excellence.

C. A. Hans is with the University of Kassel, Automation and Sensorics in Networked Systems Group, Germany.

E-mail: {sterle, raisch}@control.tu-berlin.de, hans@uni-kassel.de

Abstract.

In this paper, a model predictive control scheme for wind farms is presented. Our approach considers wake dynamics including their influence on local wind conditions and allows the tracking of a given power reference. In detail, a Gaussian wake model is used in combination with observation points that carry wind condition information. This allows the estimation of the rotor effective wind speeds at downstream turbines, based on which we deduce their power output. Through different approximation methods, the associated finite horizon nonlinear optimization problem is reformulated in a mixed-integer quadratically-constrained quadratic program fashion. By solving the reformulated problem online, optimal yaw angles and axial induction factors are found. Closed-loop simulations indicate good power tracking capabilities over a wide range of power setpoints while distributing wind turbine infeed evenly among all units. Additionally, the simulation results underline real time capabilities of our approach.

1. Introduction

In state-of-the-art wind farm control, actuation is computed based on open-loop control schemes which are typically deduced via offline optimizations using steady-state models [1]. Such approaches may find optimal steady-state solutions for constant wind conditions and power setpoints. However, state and input trajectories driving the system from one state to another can lead to poor performance. Closed-loop control concepts that are designed based on dynamic models bear the potential to improve the overall performance by finding more suitable trajectories under changing wind conditions and power setpoints.

In literature, a variety of closed-loop control approaches have been studied. In [2], a control scheme which employs partial differential equations to model wakes is investigated. However, time dependencies on the thrust coefficient, which have critical influence on wake dynamics, are neglected. Additionally, the wake model is based on the Jensen model [3], which is typically less accurate than recent engineering models such as Gaussian wake models [4] or cumulative curl models [5]. In [6], a gain-scheduling proportional-integral controller for power tracking is studied. While this approach reduces mechanical stress in the presence of changing power setpoints, its power tracking capabilities are limited by the induction control range of each turbine since

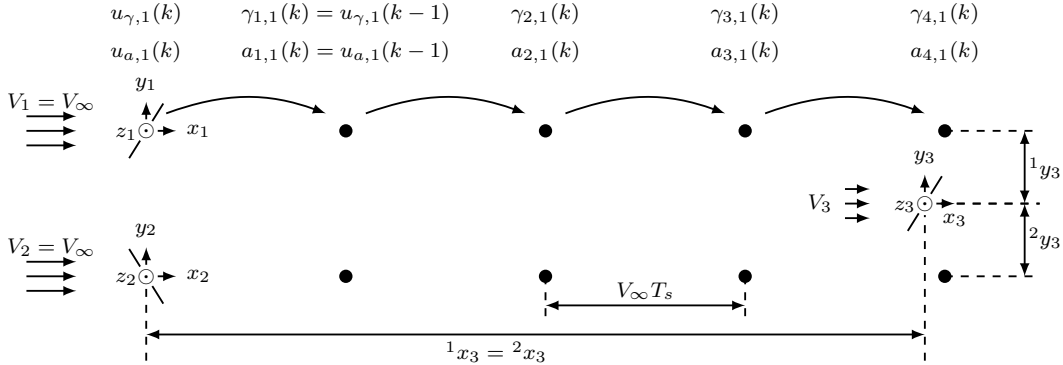


Figure 1: Simple example of a wind farm with three turbines and local coordinate systems. The solid circles represent observation points and the empty circles represent wind turbines.

yawing is not taken into account, even though it enables a larger range of available power [7–9]. In [10, 11], the framework FLORIDyn is investigated. FLORIDyn models wake dynamics by propagating wind conditions which can be influenced by turbines via observation points (OPs). However, the approach is targeted towards simulation and cannot be directly used for control.

This paper presents a novel model predictive control (MPC) approach that uses a Gaussian wake model in tandem with the concepts from [10, 11] to formulate a mixed-integer quadratically-constrained quadratic program (MIQCQP). The resulting controller is capable of finding state and input trajectories to track changing power setpoints by actively controlling wakes. A proof-of-concept case study validates our approach which provides a broad basis for more complex MPC schemes that consider, e.g., power tracking under heterogeneous wind conditions.

The remainder of this paper is structured as follows. In Section 2, wake and turbine models are introduced. Then, in Section 3, these models are used to formulate an MPC scheme. In Section 4, a case study is presented. Finally, in Section 5, the results of this paper are discussed and an outlook on future work is given.

2. Model

In this section, a control-oriented wind farm model composed of wake transport dynamics, Gaussian wake models and wind turbine (WT) model is presented. Throughout this paper, the simple wind farm in Fig. 1 serves as an example. However, the results can also be applied to more complex real-world setups. We start with some general assumptions and remarks.

Assumption 1. We assume a persistence forecast of free wind conditions, i.e., within the finite prediction horizon of the controller, the free wind speed, $V_\infty \in \mathbb{R}_{\geq 0}$, is constant in magnitude and direction.

To describe spatial quantities, each WT is equipped with a three-dimensional Cartesian coordinate system. Ass. 1 allows us to align the x -axis of each coordinate system with the free wind direction. Heights are represented by the z -coordinate, and the y -axis is perpendicular to the x - and z -axis. We refer to x, y, z directions as streamwise, spanwise and vertical, respectively. The origin of each coordinate system, where $x = y = z = 0$, is located at the centre of each WT’s rotor.

Assumption 2. For simplicity, all WTs are assumed to be identical such that they share equal parameters, e.g, diameters, hub height etc.

The following model aims to estimate the power output of each WT, which depends on their rotor effective wind speeds. As indicated in Fig. 1, the rotor effective wind speed of each upstream

WT equals the free wind speed. Since wind conditions at downstream WTs are influenced by wake, we need to model how actions of upstream WTs propagate through the wind field using transport dynamics.

2.1. Transport Dynamics

The modelling of wake transport dynamics sketched in Fig. 1 is inspired by FLORIDyn [10–12]. Let $k \in \mathbb{N}_0$ denote the discrete time instant. Then, consider WT i with control inputs in the form of yaw misalignment $u_{\gamma,i}(k) \in \mathbb{R}$ and axial induction factor $u_{a,i}(k) \in \mathbb{R}_{>0}$, which is short for $u_{\gamma,i}(kT_s)$ and $u_{a,i}(kT_s)$, where $T_s \in \mathbb{R}_{>0}$ denotes the controller sampling time. The axial induction factor is a measurement for how strongly a WT decelerates the flow field (as long as it is below 0.4, see, e.g., [13]). Massless particles, called observation points (OPs), are placed behind WT i in a distance of $V_\infty T_s$ in streamwise direction. Each OP m associated with WT i exhibits a yaw misalignment $\gamma_{m,i}(k) \in \mathbb{R}$ and an axial induction factor $a_{m,i}(k) \in \mathbb{R}_{\geq 0}$ which allow to approximate local wind conditions.

Assumption 3. The local wind conditions are assumed to propagate with velocity V_∞ .

Ass. 3 allows us to update each OP at each time step either with the values of its upstream OP or the values originating from the associated WT. Let $N_{OP} \in \mathbb{N}$ denote the number of OPs per turbine. Then, the values of the OPs of WT i , collected in $\gamma_i = [\gamma_{1,i}, \gamma_{2,i}, \dots, \gamma_{N_{OP},i}]^T$ and $a_i = [a_{1,i}, a_{2,i}, \dots, a_{N_{OP},i}]^T$ can be described by the dynamics

$$\gamma_i(k+1) = A\gamma_i(k) + Bu_{\gamma,i}(k), \quad (1a)$$

$$a_i(k+1) = Aa_i(k) + Bu_{a,i}(k). \quad (1b)$$

Here, $A \in \mathbb{R}^{N_{OP} \times N_{OP}}$ as well as $B \in \mathbb{R}^{N_{OP}}$ are given by

$$A = \begin{bmatrix} 0 & 0 & \dots & 0 \\ 1 & 0 & \dots & 0 \\ & \ddots & \ddots & \vdots \\ 0 & & & 1 & 0 \end{bmatrix} \quad \text{and} \quad B = [1 \ 0 \ \dots \ 0]^T.$$

The OP closest to each downstream WT will then be used to estimate local wind conditions for the respective WT using the following wake model.

2.2. Gaussian Wake Model

In this section, the Gaussian wake model from [4], which is used to estimate local wind conditions, will be recalled. The defining parameters are sketched in Fig. 2.

For simplicity, subscripts for the yaw misalignment and axial induction factor are omitted in this section. Thus, consider an OP with yaw misalignment γ and axial induction factor a . Then, its associated thrust coefficient $C_t \in \mathbb{R}_{>0}$ is

$$C_t(\gamma, a) = 4a(1 - a \cos(\gamma)). \quad (2)$$

The wake core length $x_c \in \mathbb{R}_{\geq 0}$ is

$$x_c(\gamma, a) = D \frac{\cos(\gamma)(1 + \sqrt{1 - C_t})}{\sqrt{2}(\alpha I + \beta(1 - \sqrt{1 - C_t}))}, \quad (3)$$

where $D \in \mathbb{R}_{\geq 0}$ denotes the WT's diameter and $\alpha, \beta \in \mathbb{R}_{\geq 0}$ are constants which describe the wake recovery rate. The wake core length marks the distance in downstream direction that separates near wake conditions ($x < x_c$) from far wake conditions for ($x \geq x_c$). This is important since different models are used to describe the flow field under these different conditions.

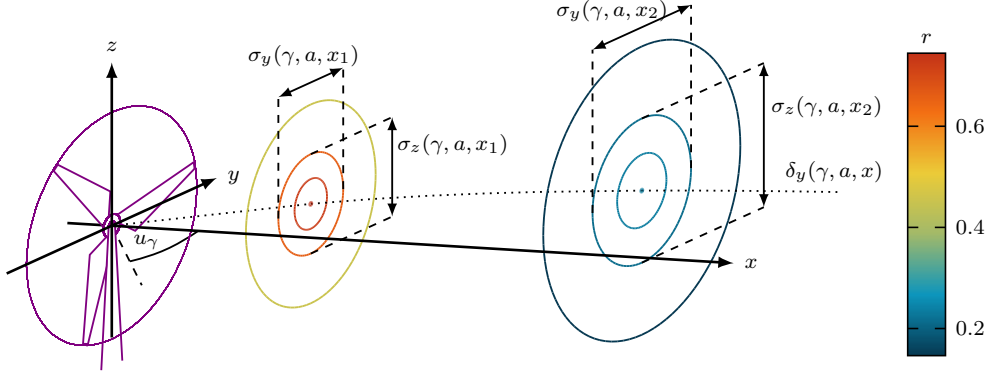


Figure 2: Three dimensional wake forms and their defining parameters. From the turbine on the left, the wake form starts with smaller wake widths, σ_y and σ_z , and higher wind speed deficit at the centre. With increasing distance in x -direction, the wake widths become larger, which leads to a flatter wind speed deficit distribution. Additionally, the centre wind speed deficit decreases. Due to the nonzero yaw misalignment, u_γ , of the WT the wake centre is deflected by δ_y .

Assumption 4. The turbulence intensity, $I \in \mathbb{R}_{\geq 0}$, is constant.

Assumption 5. Streamwise distances between turbines are much larger than their diameters, such that far wake conditions can be considered at all downstream turbines. Consequently, we can assume $x \geq x_c$.

At far wake conditions, the local wind speed deficit $r \in \mathbb{R}_{\geq 0}$ can be described by [4]

$$r(\gamma, a, x, y, z) = r_c(\gamma, a, x) \exp\left(-\left(\frac{y - \delta_y(\gamma, a, x)}{\sqrt{2}\sigma_y(\gamma, a, x)}\right)^2\right) \exp\left(-\left(\frac{z}{\sqrt{2}\sigma_z(\gamma, a, x)}\right)^2\right). \quad (4)$$

The spanwise and vertical wake widths, $\sigma_y, \sigma_z \in \mathbb{R}_{\geq 0}$, are given by

$$\sigma_y(\gamma, a, x) = k_y(x - x_c(\gamma, a)) + \frac{D}{\sqrt{8}} \cos(\gamma), \quad (5a)$$

$$\sigma_z(\gamma, a, x) = k_z(x - x_c(\gamma, a)) + \frac{D}{\sqrt{8}}, \quad (5b)$$

where $k_y = k_z \in \mathbb{R}_{\geq 0}$ describe spanwise and vertical wake growth rates which linearly depend on the turbulence intensity. Moreover, the wind speed deficit at the wake centre is

$$r_c(\gamma, a, x) = 1 - \sqrt{1 - \frac{D^2 C_t(\gamma, a) \cos(\gamma)}{8\sigma_y(\gamma, a, x)\sigma_z(\gamma, a, x)}}. \quad (6)$$

Finally, the wake centre's spanwise deflection is given by

$$\delta_y(\gamma, a, x) = \zeta(\gamma, a)x_c + D \frac{\zeta(\gamma, a)}{14.7} \sqrt{\frac{\cos(\gamma)}{k_y k_z C_t(\gamma, a)}} \left(2.9 + 1.3\sqrt{1 - C_t(\gamma, a)} - C_t(\gamma, a)\right) \ln\left(\frac{(1.6 + \sqrt{C_t(\gamma, a)})\left(1.6\sqrt{\frac{8\sigma_y(\gamma, a, x)\sigma_z(\gamma, a, x)}{D^2 \cos(\gamma)}} - \sqrt{C_t(\gamma, a)}\right)}{(1.6 - \sqrt{C_t(\gamma, a)})\left(1.6\sqrt{\frac{8\sigma_y(\gamma, a, x)\sigma_z(\gamma, a, x)}{D^2 \cos(\gamma)}} + \sqrt{C_t(\gamma, a)}\right)}\right), \quad (7)$$

with skew angle

$$\zeta(\gamma, a) = \frac{0.3\gamma}{\cos(\gamma)} \left(1 - \sqrt{1 - C_t(\gamma, a) \cos(\gamma)}\right). \quad (8)$$

Eqs. (2) to (8) can now be employed to calculate local wind conditions at downstream WTs.

2.3. Wind Turbine Model

Assumption 6. We expect the turbine dynamics to be significantly faster than the farm dynamics described in (1). Therefore, the WT dynamics can be neglected. However, the yaw misalignment's rate of change is assumed to be limited.

In the following, we focus on estimating generated power for given local wind conditions. Since each downstream turbine is influenced by wakes we first require the rotor effective wind speed which we will deduce via the local wind speed deficit (4). Consider an OP with yaw-misalignment γ and axial induction factor a which is associated with WT i . This OP is located close to a downstream WT j with yaw misalignment $u_{\gamma,j}$ which has the i -coordinates $({}^i x_j, {}^i y_j, {}^i z_j)$ (compare Fig. 1). The local wind speed deficit that originates from WT i is described by $r_i(\gamma, a, {}^i x_j, {}^i y_j, {}^i z_j)$. To compute the rotor effective wind speed deficit $R_{i,j}(\gamma, a, {}^i x_j, {}^i y_j, u_{\gamma,j})$, we need to integrate $r_i(\gamma, a, {}^i x_j, {}^i y_j, {}^i z_j)$ along WT j 's rotor surface and divide the result by its surface area (see Fig. 3).

Assumption 7. The yaw misalignment is limited to $u_{\gamma,i} \in [-\pi/6, \pi/6]$ (see, e.g., [14]).

We can describe any point p in the surface area of WT j 's rotor disc with $l \in [0, D/2]$ and $\phi \in [0, 2\pi)$. Then, with Ass. 7, we can deduce $|l \sin(u_{\gamma,j}) \cos(\phi)| \leq |D/2 \sin(\pi/6) \cos(0)| = D/4$. With $D/4 \ll {}^i x_j$ (recall Ass. 5), the following approximation is justified:

$$p = \begin{bmatrix} {}^i x_j + l \sin(u_{\gamma,j}) \cos(\phi) \\ {}^i y_j + l \cos(u_{\gamma,j}) \cos(\phi) \\ l \sin(\phi) \end{bmatrix} \approx \begin{bmatrix} {}^i x_j \\ {}^i y_j + l \cos(u_{\gamma,j}) \cos(\phi) \\ l \sin(\phi) \end{bmatrix}, \quad (9)$$

To compute $R_{i,j}(\gamma, a, {}^i x_j, {}^i y_j, u_{\gamma,j})$ by integrating $r_i(\gamma, a, {}^i x_j, {}^i y_j, {}^i z_j)$ over l and ϕ , the Jacobian determinant is needed. Since the x -component is considered constant in (9), the Jacobian determinant is given by

$$\det \left(\frac{\partial(p_y, p_z)}{\partial(l, \phi)} \right) = \det \left(\begin{bmatrix} \cos(u_{\gamma,j}) \cos(\phi) & -l \cos(u_{\gamma,j}) \sin(\phi) \\ \sin(\phi) & l \cos(\phi) \end{bmatrix} \right) = l \cos(u_{\gamma,j}). \quad (10)$$

With this, we can deduce

$$R_{i,j}(\gamma, a, {}^i x_j, {}^i y_j, u_{\gamma,j}) = \frac{\int_0^{2\pi} \int_0^{D/2} r_i(\gamma, a, {}^i x_j, {}^i y_j + l \cos(u_{\gamma,j}) \cos(\phi), l \sin(\phi)) l \cos(u_{\gamma,j}) dl d\phi}{\int_0^{2\pi} \int_0^{D/2} l \cos(u_{\gamma,j}) dl d\phi} \quad (11a)$$

$$= \frac{4}{\pi D^2} \int_0^{2\pi} \int_0^{D/2} r_i(\gamma, a, {}^i x_j, {}^i y_j + l \cos(u_{\gamma,j}) \cos(\phi), l \sin(\phi)) l dl d\phi. \quad (11b)$$

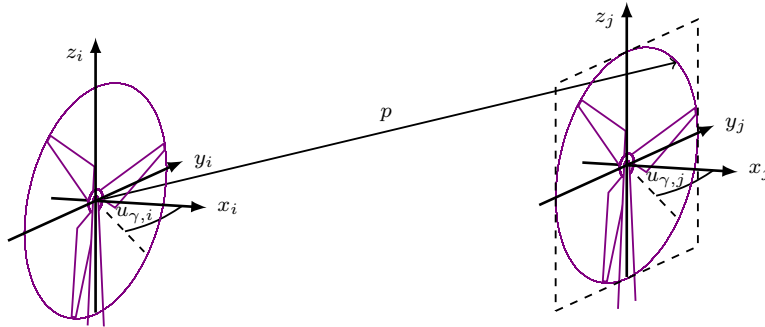


Figure 3: Point on downstream WT rotor disc and rectangular approximation.

This integral, however, is hard to solve analytically. Therefore, we approximate it by using a $D \times D \cos(u_{\gamma,j})$ rectangle, instead (see Fig. 3), i.e.,

$$R_{i,j}(\gamma, a, {}^i x_j, {}^i y_j, u_{\gamma,j}) \approx \frac{1}{D^2 \cos(u_{\gamma,j})} \int_{-\frac{1}{2}D}^{\frac{1}{2}D} \int_{{}^i y_j - \frac{1}{2}D \cos(u_{\gamma,j})}^{{}^i y_j + \frac{1}{2}D \cos(u_{\gamma,j})} r_i(\gamma, a, {}^i x_j, y, z) dy dz, \quad (12a)$$

$$= \frac{\pi r_C \sigma_y \sigma_z}{D^2 \cos(u_{\gamma,j})} \left(\operatorname{erf} \left(\frac{{}^i y_j + \frac{1}{2}D \cos(u_{\gamma,j}) - \delta_y}{\sqrt{2} \sigma_y} \right) - \operatorname{erf} \left(\frac{{}^i y_j - \frac{1}{2}D \cos(u_{\gamma,j}) - \delta_y}{\sqrt{2} \sigma_y} \right) \right) \operatorname{erf} \left(\frac{1}{\sqrt{8}} \frac{D}{\sigma_z} \right), \quad (12b)$$

where $\operatorname{erf}(t)$ denotes the error function which is defined as $\frac{2}{\sqrt{\pi}} \int_0^t \exp(-\tau^2) d\tau$.

Let the set $\mathbb{U}_j \subset \mathbb{N}$ contain all WTs i that affect WT j . Motivated by [11], the rotor effective wind speed V_j at WT j is calculated as

$$V_j = V_\infty \prod_{i \in \mathbb{U}_j} (1 - R_{i,j}). \quad (13)$$

Now that we have the rotor effective wind speeds, we can deduce the power output of each WT i via

$$P_i = \frac{\eta \rho \pi D^2}{8} V_i^3 C_{p,i}(u_{a,i}) \cos(u_{\gamma,i})^{p_p}, \quad (14)$$

where $\eta \in \mathbb{R}_{\geq 0}$ denotes the WT's efficiency, $\rho \in \mathbb{R}_{\geq 0}$ the air density and $p_p \in \mathbb{R}_{\geq 0}$ the power-yaw loss exponent [13, 15]. In literature, various numbers for p_p have been reported. For instance, [16] reports $p_p = 2.1$, [17, 18] $p_p = 3$ and [19] $p_p = 1.8$. As a middle ground, in this work, $p_p = 2$ is chosen. The power coefficient $C_{p,i} \in \mathbb{R}$ [13] is given by

$$C_{p,i}(u_{a,i}) = 4\kappa u_{a,i} (1 - u_{a,i})^2, \quad (15)$$

where $\kappa \in \mathbb{R}$ is a correction factor to account for the fact that real rotor discs are not ideal. Finally, the power generated by the farm can be deduced by summing over all N_T WTs, i.e.,

$$P_F = \sum_{i=1}^{N_T} P_i. \quad (16)$$

3. Model Predictive Control

Using the model from Section 2, the behaviour of the wind farm can be predicted over a finite horizon based on the current state of the system. In what follows, predicted signals are denoted with the time index $(n|k)$, where $n \in [k, k + N_p]$ with $N_p \in \mathbb{N}$ being the controller's prediction horizon. In this notation, k marks the current discrete time instant, whereas n denotes the prediction time instant.

Assumption 8. The states in (1) are available at time k such that $\gamma_i(k|k) = \gamma_i(k)$ and $a_i(k|k) = a_i(k)$. This can be achieved using, e.g., the FLORIDyn based concept presented in [20].

For $u_{a,i}$, we demand

$$0.06 \leq u_{a,i}(n|k) \leq 0.33 \quad (17a)$$

for all $i \in [1, N_T]$. These bounds are chosen for two reasons. (1) the blade element momentum theory [13] is only valid for $0 < u_{a,i} \leq 0.4$. (2) the power coefficient $C_{p,i}(u_{a,i})$ is at its maximum value for $u_{a,i} = 0.33$. We can reduce $C_{p,i}$ by either increasing $u_{a,i}$ above 0.33 or by decreasing it. Since C_t is related to the thrust force acting on the rotor, which again is associated with mechanical stress, lower values for $u_{a,i}$ are preferable as they lead to lower values of C_t . The lower bound is chosen as a margin to obtain solutions that keep $C_t > 0$.

Based on Ass. 7, we introduce the box constraint

$$-\pi/6 \leq u_{\gamma,i}(n|k) \leq \pi/6 \quad (17b)$$

for all $i \in [1, N_T]$. Additionally, we have the constraint

$$-\Delta u_\gamma \leq u_{\gamma,i}(n|k) - u_{\gamma,i}(n-1|k) \leq \Delta u_\gamma \quad (18)$$

for all $i \in [1, N_T]$ to account for the limited yaw actuation speed. Note, that we do not implement an analogous constraint for $u_{a,i}$ since this part of the WT dynamics is expected to be negligible (recall Ass. 6). During power tracking, we expect lower values of $u_{a,i}$ for which x_c in (3) becomes larger. To uphold Ass. 5, we employ

$$x_c(n|k) \leq x_j \quad (19)$$

for all $j \in [1, N_T]$ and $i \in \mathbb{U}_j$ so that we have far wake conditions at downstream WTs. Finally, we want to limit all power outputs by the WTs' rated power $P_r \in \mathbb{R}_{\geq 0}$, i.e.,

$$P_i(n|k) \leq P_r. \quad (20)$$

We choose the cost function

$$\ell(k) = \sum_{n=k}^{k+N_p} \left(q_P (P_F(n|k) - P_{ref}(k))^2 + q_{P,2} \sum_i^{N_T} P_i(n|k)^2 \right) \quad (21)$$

with weightings $q_P, q_{P,2} \in \mathbb{R}_{>0}$. The cost function aims to track the reference power $P_{ref}(k)$ and to distribute the farm power evenly among all WTs. Let us define the control matrix

$$U_i(k) = \begin{bmatrix} u_{\gamma,i}(k|k) & u_{\gamma,i}(k+1|k) & \cdots & u_{\gamma,i}(k+N_p|k) \\ u_{a,i}(k|k) & u_{a,i}(k+1|k) & \cdots & u_{a,i}(k+N_p|k) \end{bmatrix} \quad (22)$$

and form $U(k) = [U_1(k), \dots, U_{N_T}(k)]$ to state the following nonlinear optimization problem.

Problem 1.

$$\min_{U(k)} \ell(k)$$

subject to

$$\begin{bmatrix} \gamma_i(n+1|k) \\ a_i(n+1|k) \end{bmatrix} = \begin{bmatrix} A & 0 \\ 0 & A \end{bmatrix} \begin{bmatrix} \gamma_i(n|k) \\ a_i(n|k) \end{bmatrix} + \begin{bmatrix} B & 0 \\ 0 & B \end{bmatrix} \begin{bmatrix} u_{\gamma,i}(n|k) \\ u_{a,i}(n|k) \end{bmatrix}$$

as well as (2), (3), (5) to (8) and (12) to (20) $\forall n \in [k, k+N_p]$ and $i \in [1, N_T]$ with given initial conditions $\gamma_i(k|k) = \gamma_i(k)$, $a_i(k|k) = a_i(k)$ and $u_{\gamma,i}(k-1|k) = u_{\gamma,i}(k-1)$ which refers to the previous yaw misalignment.

The solutions obtained for $u_{\gamma,i}(k|k)$ and $u_{a,i}(k|k)$ are used to actuate the wind farm. At $k+1$, new initial values are available and the process is repeated to account for disturbances and model inaccuracies which gives us a moving horizon control scheme.

Problem 1 is a nonlinear optimization problem. While nonlinear solvers are available, they may perform poorly in terms of solving times and may not find a globally optimal solution. Since we are interested in real-time control, we will reformulate Problem 1 as an MIQCQP for which the global optimum can be found by commercial solvers in reasonable time.

Constraint (17b) allows us to employ the second order Taylor approximations

$$\cos(u_{\gamma,i}) \approx 1 - \frac{u_{\gamma,i}^2}{2} \quad (23) \quad \text{and} \quad \frac{1}{\cos(u_{\gamma,i})} \approx 1 + \frac{u_{\gamma,i}^2}{2}. \quad (24)$$

The wake core length x_c (3), wake centre's wind speed deficit r_C (6) and wake centre's spanwise deflection δ_y (7) are approximated by polynomials in γ and a . This yields

$$x_c(\gamma, a) = K_{20}^{x_c} \gamma^2 + K_{02}^{x_c} a^2 + K_{01}^{x_c} a + K_{00}^{x_c}, \quad (25)$$

where $K_{00}^{x_c}, K_{01}^{x_c}, K_{02}^{x_c}, K_{20}^{x_c} \in \mathbb{R}$ are precomputed based on wind conditions. For r_C and δ_y , the resulting polynomials are

$$r_C(\gamma, a) = K_{03}^C a^3 + K_{21}^C \gamma^2 a + K_{20}^C \gamma^2 + K_{02}^C a^2 + K_{01}^C a + K_{00}^C \quad (26)$$

$$\delta_y(\gamma, a) = K_{30}^{\delta_y} \gamma^3 + K_{12}^{\delta_y} \gamma a^2 + K_{11}^{\delta_y} \gamma a + K_{10}^{\delta_y} \gamma, \quad (27)$$

where the polynomial coefficients, e.g., $K_{03}^C, K_{00}^{\delta_y}$, depend on the farm's geometry and are computed offline yielding approximation errors below 17% for turbine distances within $[5D, 15D]$. To reformulate the remaining equations, auxiliary variables and additional equality constraints are introduced which are displayed by Table 1.

Finally, the function $\text{erf}(\xi)$ is approximated by a piecewise affine function $\text{erf}^{PWA}(\xi)$ (see also [21, 22]). These changes allow us to reformulate Problem 1 as the following MIQCQP.

Problem 2.

$$\min_{U(k)} \ell(k)$$

subject to

$$\begin{bmatrix} \gamma_i(n+1|k) \\ a_i(n+1|k) \end{bmatrix} = \begin{bmatrix} A & 0 \\ 0 & A \end{bmatrix} \begin{bmatrix} \gamma_i(n|k) \\ a_i(n|k) \end{bmatrix} + \begin{bmatrix} B & 0 \\ 0 & B \end{bmatrix} \begin{bmatrix} u_{\gamma,i}(n|k) \\ u_{a,i}(n|k) \end{bmatrix}$$

as well as (16) to (20) and (23) to (27) and Table 1 $\forall n \in [k, k + N_p]$ and $i \in [1, N_T]$ with given initial conditions $\gamma_i(k|k) = \gamma_i(k)$, $a_i(k|k) = a_i(k)$ and $u_{\gamma,i}(k-1|k) = u_{\gamma,i}(k-1)$.

4. Case Study

In what follows, Problem 2 will be used to operate the farm in Fig. 1. The MPC and farm parameters, which are based on IEA 3.4MW turbines [23] are displayed in Table 2. The

Table 1: auxiliary variables

Original term	Quadratic reformulation	Original term	Quadratic reformulation
$\cos(u_\gamma)$	$\xi_1 = 1 - \frac{u_\gamma}{2}$	$\frac{i y_j + \frac{1}{2} D \cos(u_{\gamma,j} - \delta_y)}{\sqrt{2} \sigma_y}$	$\xi_{11} \sqrt{2} \sigma_y = i y_j + \frac{1}{2} D \xi_1 - \delta_y$
γ^2	$\xi_2 = \gamma^2$	$\frac{i y_j - \frac{1}{2} D \cos(u_{\gamma,j} - \delta_y)}{\sqrt{2} \sigma_y}$	$\xi_{12} \sqrt{2} \sigma_y = i y_j - \frac{1}{2} D \xi_1 - \delta_y$
γ^3	$\xi_3 = \xi_2 \gamma$	$\frac{D}{\sqrt{8} \sigma_z}$	$\xi_{13} \sqrt{8} \sigma_z = D$
a^2	$\xi_4 = a^2$	$r_C \sigma_y$	$\xi_{14} = r_C \sigma_y$
a^3	$\xi_5 = \xi_4 a$	$r_C \sigma_y \sigma_z$	$\xi_{15} = \xi_{14} \sigma_z$
$(1 - u_a)^2$	$\xi_6 = (1 - u_a)^2$	$\frac{\pi r_C \sigma_y \sigma_z}{D^2 \cos(u_\gamma)}$	$\xi_{16} D^2 = \xi_{15} \pi (2 - \xi_1)$
C_p	$\xi_7 = \kappa 4 u_a \xi_6$	$\frac{\pi r_C \sigma_y \sigma_z}{D^2 \cos(u_\gamma)} \text{erf}\left(\frac{D}{\sqrt{8} \sigma_z}\right)$	$\xi_{17} = \xi_{16} \text{erf}^{PWA}(\xi_{13})$
V^2	$\xi_8 = V^2$	r_C	$\xi_{18} (\text{erf}^{PWA}(\xi_{11}) - \text{erf}^{PWA}(\xi_{12}))$
V^3	$\xi_9 = \xi_8 V$	$\cos(u_\gamma)^{p_p}$	$\xi_{19} = \xi_1^2$
$C_p V^3$	$\xi_{10} = \xi_7 \xi_9$	P	$\xi_{20} = \frac{\eta \pi D^2}{8} \xi_{18} \xi_{19}$

Table 2: farm and controller parameters

Parameter	Value	Parameter	Value	Parameter	Value	Parameter	Value
T_s	13 s	V_∞	10 m/s	D	130 m	ρ	1.225 kg/m ³
I	6 %	k_y, k_z	0.0267	η	0.9367	P_r	3.35 MW
N_p	8	κ	0.8174	Δu_γ	0.0572	$^1 y_3$	-0.75D
$^2 y_3$	0.75D	q_P	10 ⁻⁸ 1/W	$^1 x_3, ^2 x_3$	7D	$q_{P,2}$	10 ⁻¹² 1/W

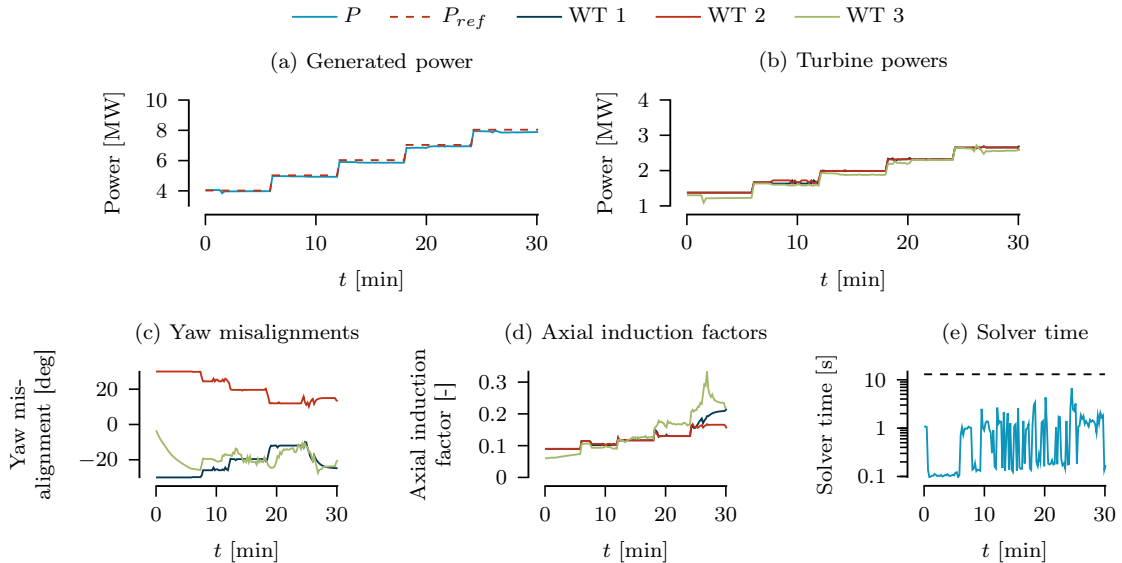


Figure 4: Simulation results for three turbine farm. The results for combined farm power, turbine power, yaw misalignment, axial induction factor and solver times are depicted. The controller’s sampling time is indicated by a dashed black line in (e).

prediction horizon N_p is chosen such that the effects of $u_{\gamma,1}$ and $u_{\gamma,2}$ on WT 3 are considered within the prediction. The MPC is implemented in MATLAB using Yalmip [24] and Gurobi. All simulations are conducted on a MacBook Air with an Apple M1 chip with 8 cores and 8 GB RAM. The wind farm is simulated using FLORIDyn .

The results in Fig. 4 indicate that the farm approximately tracks the reference power while evenly distributing infeed among all WTs, which indicates that mechanical loads are also well distributed. To achieve lower power outputs, the upstream WTs’ yaw misalignments are set such that wakes are steered towards WT 3 and its available power is reduced. With increasing reference power the yaw misalignments are updated such that the wakes are steered away from WT 3 to increase its available power. Thus, higher power outputs can be achieved. The axial induction factors are not evenly distributed among all turbines. While those of WT 1 and 2 appear similar, the one of WT 3 differs to compensate wake effects. Its noticeable that the yaw misalignment of WT 3 is further used to control its power output as no other turbine is affected by its wake. Finally, the solver time in Fig. 4 (e) remains below the sampling time during the simulation which indicates real-time applicability of the MPC.

5. Conclusions

In this paper, a mixed-integer quadratically-constrained quadratic model predictive wind farm controller was presented. Our model based approach considers time-dependent wake dynamics. We could show that our approach is capable of approximately tracking a given reference power over a large range by combining induction control and yaw misaligning. Additionally, the power output is evenly distributed between each turbine.

The presented controller provides a basis for wake modelling receding horizon control schemes. Further research shall investigate options to keep the mechanical loads evenly distributed and lift some assumptions such as static wind conditions and the far wake limitation (Ass. 1 and 3 to 5). Furthermore, the controller shall be tested on more complex wind farm topologies and in high-fidelity simulations such as SOWFA to further validate its real world applicability. Finally, the wind farm controller shall be employed with individual wind turbine controllers, e.g., from [25].

6. Literature

- [1] J. Meyers, C. Bottasso, K. Dykes, P. Fleming, P. Gebraad, G. Giebel, T. Göçmen, and J.-W. van Wingerden, “Wind farm flow control: prospects and challenges,” *Wind Energy Science*, vol. 7, 2022.
- [2] C. R. Shapiro, P. Bauweraerts, J. Meyers, C. Meneveau, and D. F. Gayme, “Model-based receding horizon control of wind farms for secondary frequency regulation,” *Wind Energy*, vol. 20, no. 7, pp. 1261–1275, 2017.
- [3] N. Jensen, *A note on wind generator interaction*, ser. Risø-M. Risø National Laboratory, 1983, no. 2411.
- [4] M. Bastankhah and F. Porté-Agel, “Experimental and theoretical study of wind turbine wakes in yawed conditions,” *Journal of Fluid Mechanics*, vol. 806, pp. 506–541, 2016.
- [5] C. J. Bay, P. Fleming, B. Doekemeijer, J. King, M. Churchfield, and R. Mudafort, “Addressing deep array effects and impacts to wake steering with the cumulative-curl wake model,” *Wind Energy Science*, 2022.
- [6] M. Vali, V. Petrović, G. Steinfeld, L. Y. Pao, and M. Kühn, “An active power control approach for wake-induced load alleviation in a fully developed wind farm boundary layer,” *Wind Energy Science*, vol. 4, no. 1, pp. 139–161, 2019.
- [7] F. Campagnolo, R. Weber, J. Schreiber, and C. L. Bottasso, “Wind tunnel testing of wake steering with dynamic wind direction changes,” *Wind Energy Science*, vol. 5, no. 4, pp. 1273–1295, 2020.
- [8] P. Fleming, J. King, E. Simley, J. Roadman, A. Scholbrock, P. Murphy, J. K. Lundquist, P. Moriarty, K. Fleming, J. van Dam, C. Bay, R. Mudafort, D. Jager, J. Skopek, M. Scott, B. Ryan, C. Guernsey, and D. Brake, “Continued results from a field campaign of wake steering applied at a commercial wind farm – part 2,” *Wind Energy Science*, vol. 5, no. 3, pp. 945–958, 2020.
- [9] E. Simley, P. Fleming, N. Girard, L. Alloin, E. Godefroy, and T. Duc, “Results from a wake-steering experiment at a commercial wind plant: investigating the wind speed dependence of wake-steering performance,” *Wind Energy Science*, vol. 6, no. 6, pp. 1427–1453, 2021.
- [10] M. Becker, D. Allaerts, and J. W. van Wingerden, “FLORIDyn - a dynamic and flexible framework for real-time wind farm control,” *Journal of Physics: Conference Series*, vol. 2265, no. 3, p. 032103, 2022.
- [11] M. Becker, B. Ritter, B. Doekemeijer, D. van der Hoek, U. Konigorski, D. Allaerts, and J.-W. van Wingerden, “The revised FLORIDyn model: implementation of heterogeneous flow and the gaussian wake,” *Wind Energy Science*, vol. 7, no. 6, pp. 2163–2179, 2022.
- [12] P. M. O. Gebraad and J. W. van Wingerden, “A control-oriented dynamic model for wakes in wind plants,” *Journal of Physics: Conference Series*, vol. 524, p. 012186, 2014.
- [13] M. Hansen, *Aerodynamics of Wind Turbines*. Sterling, VA: Routledge, 2015.
- [14] Á. Jiménez, A. Crespo, and E. Migoya, “Application of a les technique to characterize the wake deflection of a wind turbine in yaw,” *Wind Energy*, vol. 13, no. 6, pp. 559–572, 2009.
- [15] J. Liew, A. M. Urbán, and S. J. Andersen, “Analytical model for the power-yaw sensitivity of wind turbines operating in full wake,” *Wind Energy Science*, vol. 5, no. 1, pp. 427–437, 2020.
- [16] F. Campagnolo, R. Weber, J. Schreiber, and C. L. Bottasso, “Wind tunnel testing of wake steering with dynamic wind direction changes,” *Wind Energy Science*, vol. 5, no. 4, pp. 1273–1295, 2020.
- [17] P. Krogstad and M. S. Adaramola, “Performance and near wake measurements of a model horizontal axis wind turbine,” *Wind Energy*, vol. 15, no. 5, pp. 743–756, 2011.
- [18] J. Bartl, F. Mühle, J. Schottler, L. Sætran, J. Peinke, M. Adaramola, and M. Hölling, “Wind tunnel experiments on wind turbine wakes in yaw: effects of inflow turbulence and shear,” *Wind Energy Science*, vol. 3, no. 1, pp. 329–343, 2018.
- [19] P. Fleming, P. M. Gebraad, S. Lee, J.-W. van Wingerden, K. Johnson, M. Churchfield, J. Michalakes, P. Spalart, and P. Moriarty, “Simulation comparison of wake mitigation control strategies for a two-turbine case: Simulation comparison of wake mitigation control strategies for a two-turbine case,” *Wind Energy*, vol. 18, no. 12, pp. 2135–2143, 2014.
- [20] M. Becker, D. Allaerts, and J.-W. van Wingerden, “Ensemble-based flow field estimation using the dynamic wind farm model floridyn,” *Energies*, vol. 15, no. 22, p. 8589, 2022.
- [21] A. Bemporad and M. Morari, “Control of systems integrating logic, dynamics, and constraints,” *Automatica*, vol. 35, no. 3, pp. 407–427, 1999.
- [22] A. Sterle, A. Grapentin, C. Hans, and J. Raisch, “Model Predictive Control of Wind Turbines with Piecewise-Affine Power Coefficient Approximation,” *IEEE CDC*, 2023.
- [23] P. Bortolotti, H. C. Tarres, K. Dykes, K. Merz, L. Sethuraman, D. Verelst, and F. Zahle, “Tea wind task 37 on systems engineering in wind energy – wp2.1 reference wind turbines,” NREL/TP-73492, International Energy Agency, Tech. Rep., 2019.
- [24] J. Löfberg, “Yalmip : A toolbox for modeling and optimization in matlab,” in *In Proceedings of the CACSD Conference*, Taipei, Taiwan, 2004.
- [25] A. Grapentin, A. Sterle, J. Raisch, and C. A. Hans, “LQ Optimal Control for Power Tracking Operation of Wind Turbines,” *IFAC World Congress*, 2023.